

NOVEL WAVEGUIDE PHOTODETECTORS ON InP WITH INTEGRATED LIGHT AMPLIFICATION

J. Piprek, D. Pasquariello, D. Lasaosa, and J. E. Bowers

Electrical and Computer Engineering Department
University of California, Santa Barbara, CA 93106

ABSTRACT

We investigate InP-based traveling-wave amplification photodetectors (TAP detectors). Such detectors have the potential to achieve simultaneously high saturation power, high speed, high responsivity, and quantum efficiencies well above one. Our detector design vertically combines a bulk InGaAs photodetector ridge region with laterally confined InGaAsP quantum wells for amplification. Initial experimental results confirm the underlying concept. Performance limitations are analyzed utilizing advanced three-dimensional device simulation and optimization options are discussed.

1. INTRODUCTION

Traveling-wave photodetectors (TWPDS) are able to simultaneously achieve large bandwidth and high responsivity. The optical power propagates perpendicular to the carrier extraction and therefore the efficiency and the carrier transit time can be tuned independently. However, the photocurrent is still limited by saturation effects at higher optical power. In order to overcome this limitation, we have recently proposed the traveling-wave amplification photodetector (TAP detector).^{1,2} The TAP detector has an integrated light amplification region, which makes it possible to maintain a nearly constant optical power level along the device. The optical power is kept below the saturation limit and very high photo currents can be achieved with long devices, higher than with any other photodetector. This is of great importance, for instance with fiber-optic analog links whose performance is often limited by optical loss. Signal amplification in our TAP detector enables net link gain.

2. DEVICE STRUCTURE AND EXPERIMENTAL RESULTS

The schematic cross section of our *npn*-device is shown in Fig. 1 and the layer structure is listed in Tab. 1. The top ridge includes an InGaAs detection layer, all other semiconductor layers exhibit a larger bandgap. Light amplification is provided by multiple InGaAsP quantum wells (QWs). The amplifier diode is operated at forward bias whereas the detector diode is reverse biased. Optical and electrical confinement in the center of the device is provided by the ridge-waveguide structure as well as by lateral under etching.

Microscopic pictures of fabricated devices are given in Figs. 2 and 3. The first figure shows the device after the etching. It demonstrates excellent etch selectivity between InGaAsP and InP. The second figure shows the final device. The coplanar microwave (CPW) probe pads are visible in the background. A lensed fiber with a spot size of 2-3 μm is used to couple light into the waveguide. The laser source is operated at 1550 nm wavelength with 440 μW output power. The measured photocurrent is plotted in Fig. 4 for a 300 μm long waveguide. It increases with the amplifier bias current, confirming the basic concept of TAP detectors. However, the magnitude of the photocurrent is below our expectations.

3. SIMULATION AND ANALYSIS

In order to analyze performance limitations with our first device generation, we utilize advanced three-dimensional (3D) device simulation software.³ The underlying theoretical models are discussed elsewhere.⁴

Figure 5 shows the band diagram at the vertical axis of the device. The common band offset ratio of $\Delta E_c/\Delta E_v = 40 : 60$ is employed at all interfaces. The conduction bands of the active layers are assumed parabolic and the non-parabolic valence bands are calculated by the two-band $\vec{k} \cdot \vec{p}$ method. The free carrier model for stimulated band-to-band transitions is employed to compute both gain

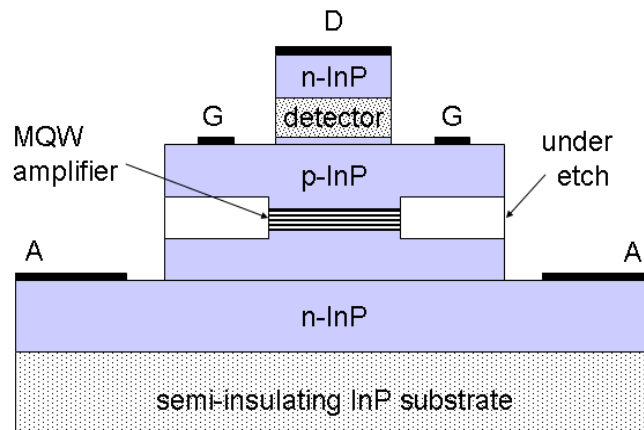


Figure 1. Cross section of the TAP detector (D - detector contact, G - ground contact, A - amplifier contact).

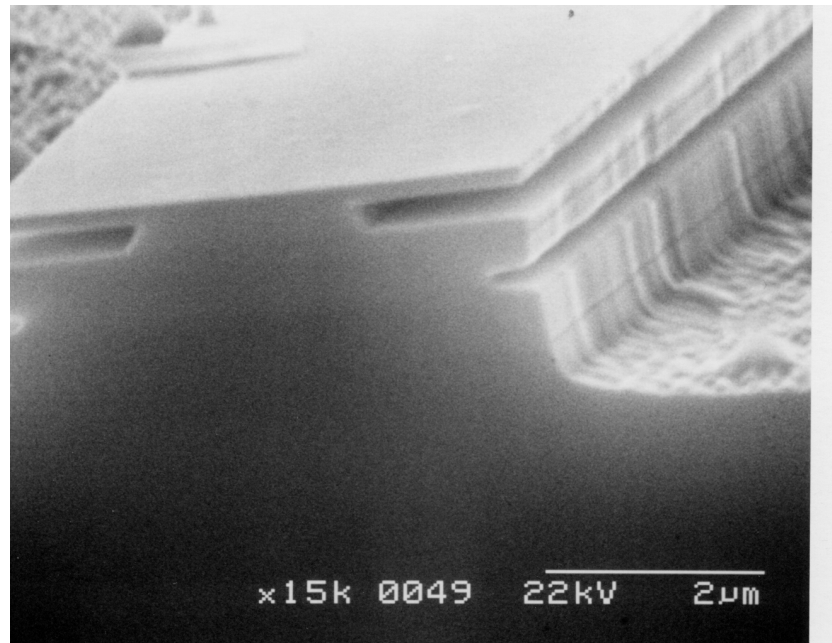


Figure 2. SEM picture of a device after undercut etching.

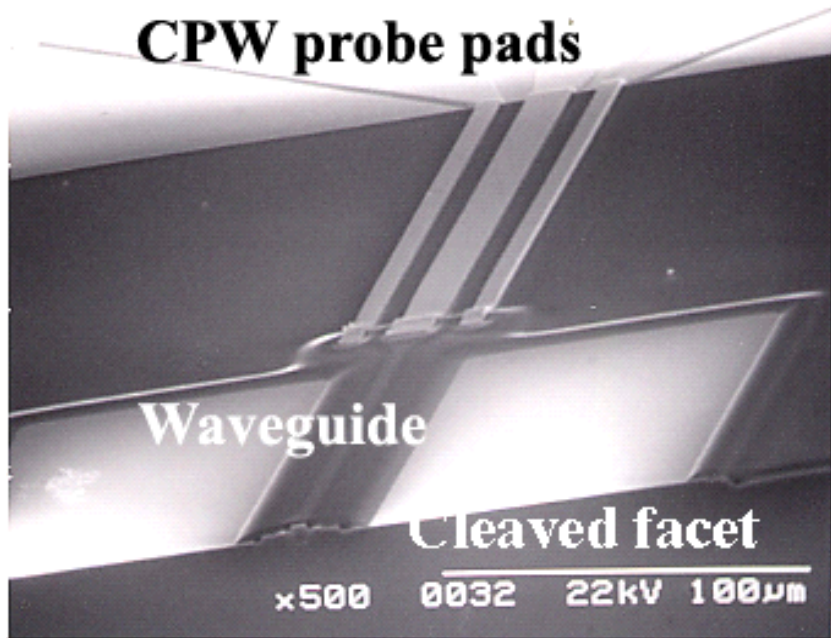


Figure 3. Microscopic picture of the final device.

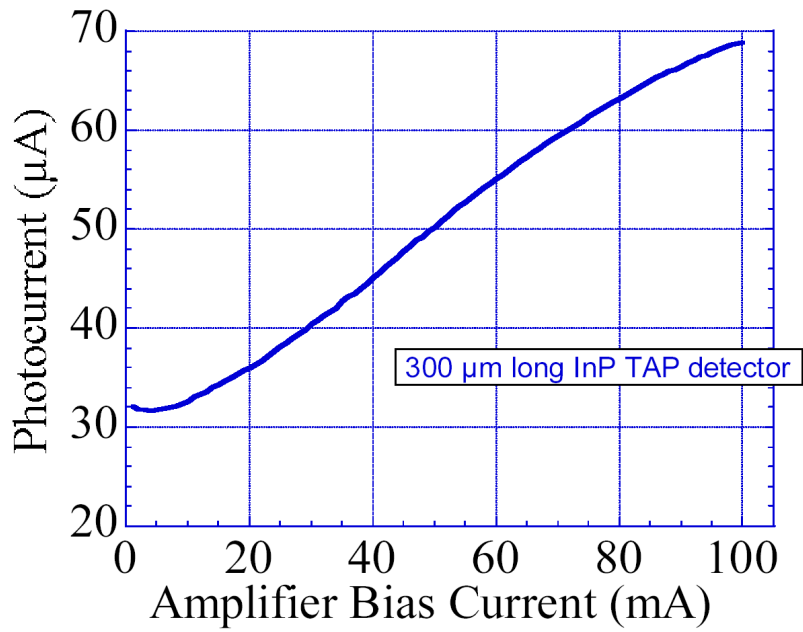


Figure 4. Measured photocurrent vs. amplifier current.

Table 1. Epitaxial layer structure of the TAP detector (l - layer thickness, N_{dop} - doping, n_r - refractive index at 1550 nm wavelength). Intrinsic (i) layers are assumed to exhibit low n-type background doping.

Parameter	l	N_{dop}	n_r
Unit	nm	$1/\text{cm}^3$	-
n-In _{0.85} Ga _{0.15} As _{0.32} P _{0.68} (D contact)	50	3×10^{18}	3.28
n-InP (cladding)	120	1×10^{18}	3.16
i-In _{0.53} Ga _{0.47} As (detector)	250	1×10^{16}	3.61
i-InP (doping offset)	200	1×10^{16}	3.16
p-InP (cladding)	200	5×10^{17}	3.16
p-InP (cladding)	50	2×10^{18}	3.16
p-In _{0.72} Ga _{0.28} As _{0.6} P _{0.4} (G contact)	100	5×10^{18}	3.40
p-InP (cladding)	50	2×10^{18}	3.16
p-InP (cladding)	200	5×10^{17}	3.16
i-InP (doping offset)	300	1×10^{16}	3.16
i-In _{0.82} Ga _{0.18} As _{0.4} P _{0.6} (waveguide)	100	1×10^{16}	3.31
i-In _{0.71} Ga _{0.29} As _{0.55} P _{0.45} (barrier)	17	1×10^{16}	3.37
i-In _{0.76} Ga _{0.24} As _{0.79} P _{0.21} (well)	7	1×10^{16}	3.62
i-In _{0.71} Ga _{0.29} As _{0.55} P _{0.45} (barrier)	8	1×10^{16}	3.37
i-In _{0.76} Ga _{0.24} As _{0.79} P _{0.21} (well)	7	1×10^{16}	3.62
i-In _{0.71} Ga _{0.29} As _{0.55} P _{0.45} (barrier)	8	1×10^{16}	3.37
i-In _{0.76} Ga _{0.24} As _{0.79} P _{0.21} (well)	7	1×10^{16}	3.62
i-In _{0.71} Ga _{0.29} As _{0.55} P _{0.45} (barrier)	8	1×10^{16}	3.37
i-In _{0.76} Ga _{0.24} As _{0.79} P _{0.21} (well)	7	1×10^{16}	3.62
i-In _{0.71} Ga _{0.29} As _{0.55} P _{0.45} (barrier)	8	1×10^{16}	3.37
i-In _{0.76} Ga _{0.24} As _{0.79} P _{0.21} (well)	7	1×10^{16}	3.62
i-In _{0.71} Ga _{0.29} As _{0.55} P _{0.45} (barrier)	8	1×10^{16}	3.37
i-In _{0.76} Ga _{0.24} As _{0.79} P _{0.21} (well)	7	1×10^{16}	3.62
i-In _{0.71} Ga _{0.29} As _{0.55} P _{0.45} (barrier)	17	1×10^{16}	3.37
i-In _{0.82} Ga _{0.18} As _{0.4} P _{0.6} (waveguide)	100	1×10^{16}	3.31
i-InP (doping offset)	50	1×10^{16}	3.16
n-InP (cladding)	400	1×10^{18}	3.16
n-In _{0.85} Ga _{0.15} As _{0.32} P _{0.68} (A contact)	100	3×10^{18}	3.28
n-InP (buffer)	300	2×10^{18}	3.16

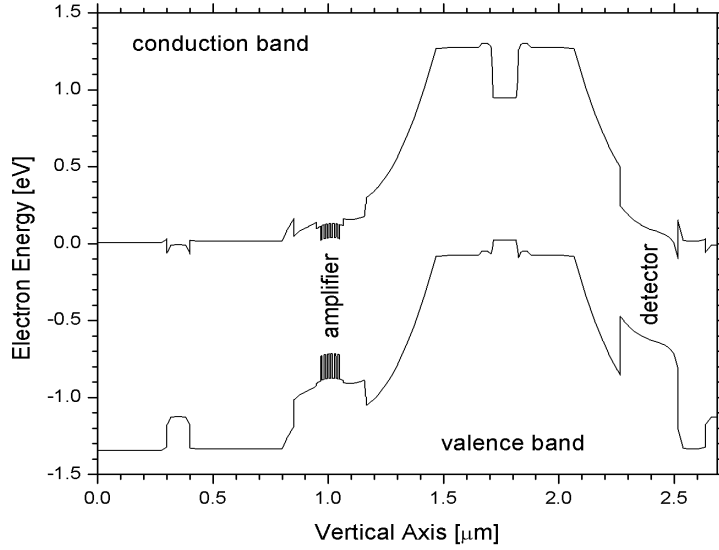


Figure 5. Vertical energy band diagram at zero bias.

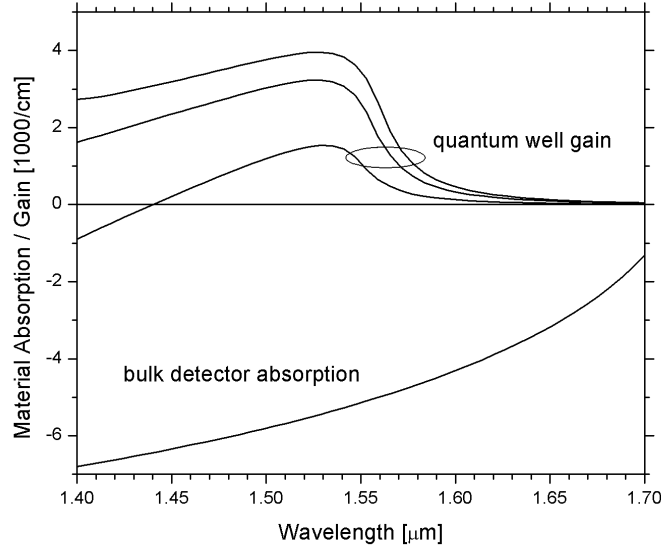


Figure 6. Gain and absorption spectra for quantum well and detector, respectively. Gain spectra are calculated at three carrier densities: $2, 4,$ and $6 \times 10^{18} \text{cm}^{-3}$, the absorption is calculated at 10^{16}cm^{-3} .

and absorption for the amplification layers and the detection layer, respectively. The calculated spectra are plotted in Fig. 6 for different carrier densities. At low carrier density (reverse bias), the bulk InGaAs detector layer exhibits an absorption coefficient of about 5000cm^{-1} at 1550nm wavelength which is reasonably close to measured values near 6000cm^{-1} . With forward bias, the carrier density in the quantum well amplification layers is much higher. At 1550nm wavelength, the gain reaches about 2500cm^{-1} for a carrier density of $4 \times 10^{18} \text{cm}^{-3}$. However, the total amplification layer thickness of 42nm is much smaller than the absorption layer thickness of 250nm . Thus, optical waveguide modes are preferred that exhibit little overlap with the detector region.

The vertical index profile of our device is plotted in Fig. 7 together with three vertical waveguide modes of interest. Mode 1 is mainly located in the detector region and mode 2 in the amplifier

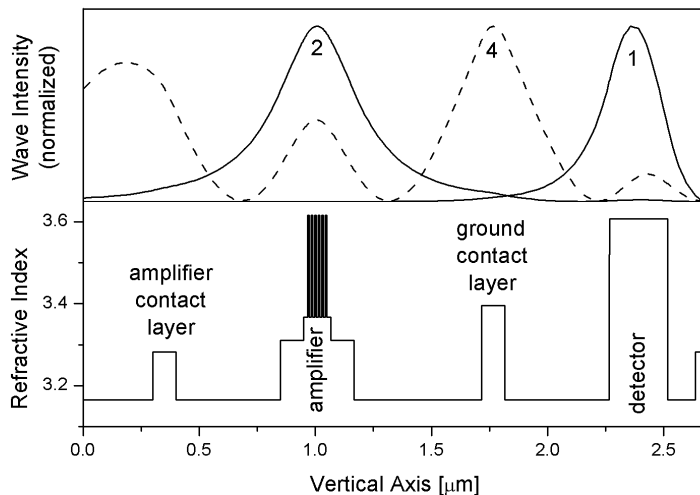


Figure 7. Vertical profile for three vertical waveguide modes (top) and for the refractive index at 1550 nm wavelength (bottom).

Mode	Γ_{amp}	Γ_{det}
1	0.00007	0.63050
2	0.07679	0.01634
4	0.01972	0.04080

Table 2. Optical confinement factors Γ_{amp} and Γ_{det} of the vertical modes in Fig. 7 for amplification and detection layers, respectively.

region. Mode 4 exhibits similar overlap with both the active regions. Mode 3 and 5 have a minimum at the MQW and they are not considered here. The optical confinement factors of the three main modes are given in Tab. 2 for both the active regions. We here assume that the etched aperture is identical to the ridge width of 2 μm . The total modal gain of each mode can be estimated as

$$g_{\text{mode}} = \Gamma_{\text{amp}}g_{\text{amp}} - \Gamma_{\text{det}}\alpha_{\text{det}} \quad (1)$$

with g_{amp} and α_{det} from Fig. 6. For a quantum well carrier density of $4 \times 10^{18} \text{cm}^{-3}$, which corresponds to about 100 mA amplifier current, the normalized modal power is given in Fig. 8 as function of travel distance. The detector mode 1 quickly decays along the waveguide, since there is no overlap with the amplifying region. Mode 4 also suffers from net absorption. Additional photons generated by stimulated recombination in the quantum wells stay within the same optical mode as the incoming photon. A balance between photon generation and absorption can only be achieved by mode 2. Relatively low pumping is sufficient to increase the optical power of mode 2 as it travels down the waveguide. Figure 9 gives a 3D plot of the mode intensity at 35 mA amplifier current.

Many different waveguide modes may be excited by coupling light into the device, e.g., from an optical fiber. Most of these modes are quickly absorbed by the thick detector region. Only those modes are useful in our device for which about the same number of photons is generated in the quantum wells and absorbed in the detector. This transfer of photons is the basic idea of the TAP detector. Partial light coupling into absorbed modes reduces the net amplification effect. Performance improvements are expected with a thinner detector layer, which would enable mode 4 to receive net gain.

The lateral current distribution is identified as another performance limiting issue. Figure 2 indicates that the lateral etching is relatively shallow in our present devices. Figure 10 shows a vector plot of the corresponding current density distribution. The p-doped ground contact layer

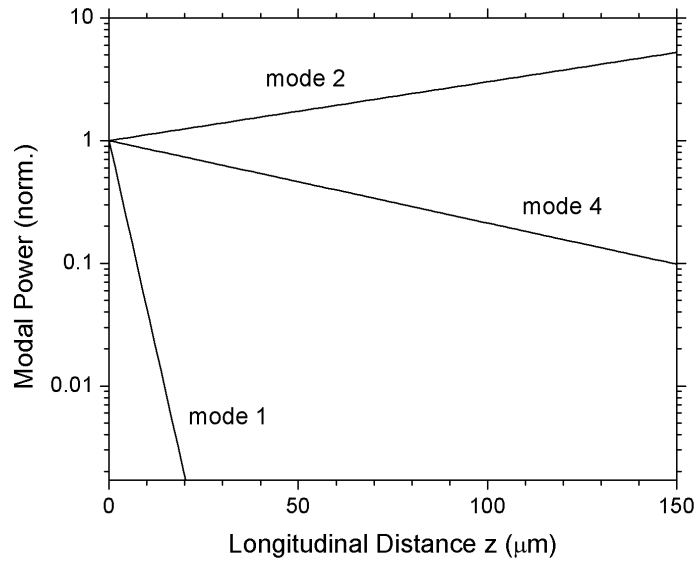


Figure 8. Normalized modal power vs. travel distance for the main three modes at 100 mA amplifier current.

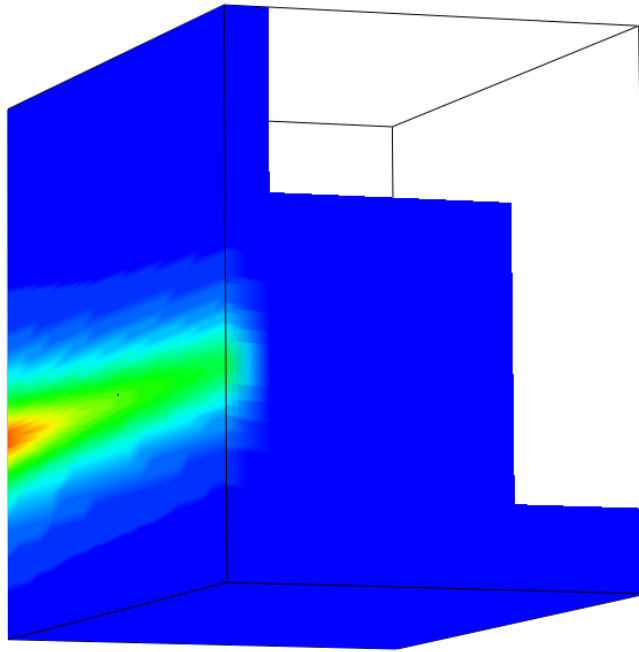


Figure 9. 3D simulation of half the device: intensity of mode 2 traveling from front to back.

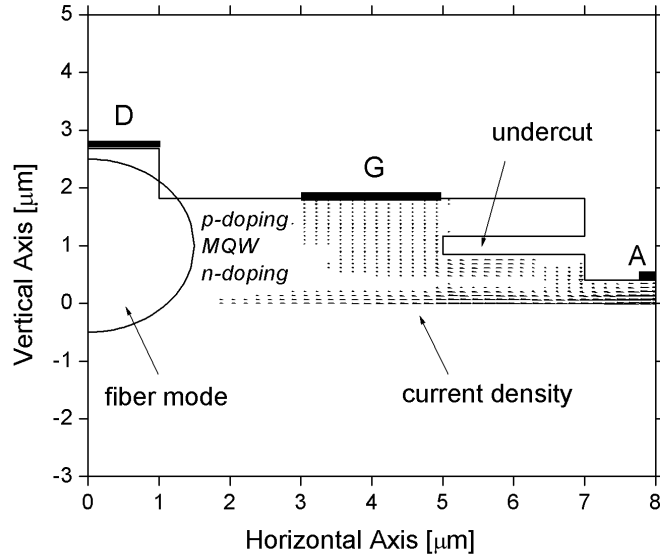


Figure 10. Calculated current density distribution with 2 μm undercut.

restricts lateral current spreading so that most of the amplifier current bypasses the optical wave in the center of the device. This results in a low quantum well carrier density near the center and in a lower modal gain than assumed above. An etched aperture similar to the ridge width is required in order to significantly enhance amplification.

4. SUMMARY

We demonstrate a first generation of InP-based traveling-wave amplification photodetectors. The measured photocurrent is relatively low. The reasons are analyzed using advanced device simulation. Part of the light is coupled into waveguide modes that are quickly absorbed without experiencing significant amplification. Only one vertical mode is identified which actually exhibits net gain. The second main problem is the lateral current distribution, which mainly bypasses the optical modes due to shallow lateral etching. Deeper under-etching and a reduced detector layer thickness are proposed in order to enhance the performance.

REFERENCES

1. D. Lasaosa, Y. J. Chiu, J. Piprek, and J. E. Bowers, "Traveling-wave amplification photodetector (TAP detector)," in *13th Lasers and Electro-Optics Society Annual Meeting*, (Piscataway), pp. 260–261, Institute of Electrical and Electronic Engineers, 2000.
2. D. Lasaosa, Y. J. Chiu, J. Piprek, and J. E. Bowers, "Modeling of traveling-wave amplification photodetectors," in *Physics and Simulation of Optoelectronic Devices IX*, Proc. SPIE 4283-64, 2001.
3. APSYS by Crosslight Software, 2001.
4. J. Piprek, *Semiconductor Optoelectronic Devices - Introduction to Physics and Simulation*. San Diego: Academic Press, 2003.